Transition State Analysis of NAD^+ Hydrolysis by the Cholera Toxin Catalytic Subunit

Kathleen A. Rising and Vern L. Schramm*

Contribution from the Department of Biochemistry, Albert Einstein College of Medicine, Bronx, New York 10461

Received June 28, 1996[⊗]

Abstract: The transition state for NAD^+ (oxidized nicotinamide adenine dinucleotide) hydrolysis by the cholera toxin A1 polypeptide (CTA) has been characterized by multiple V/K kinetic isotope effects (KIEs) using labeled NAD^+ as the substrate. CTA causes cholera by catalyzing the ADP-ribosylation of the signal-transducing $G_{s\alpha}$ protein. *In vitro*, CTA catalyzes the ADP-ribosylation of several simple guanidino compounds as well as the slow hydrolysis of NAD^+ ($k_{cat} = 8\ min^{-1}$, $K_m = 14$ mM) to form ADP−ribose and nicotinamide. KIEs for NAD^+ hydrolysis are the following: primary $^{14}C = 1.030 \pm 0.005$, primary $^{15}N = 1.029 \pm 0.004$, α-secondary $^3H = 1.186 \pm 0.004$, β-secondary $^3H = 1.108 \pm 0.004$, γ-secondary $^3H = 0.986 \pm 0.003$, δ-secondary $^3H = 1.020 \pm 0.003$, and primary double $= 1.052 \pm 0.004$. On the basis of steady-state kinetic parameters for CTA-catalyzed NAD^+ hydrolysis, as well as a comparison with KIEs measured for NAD^+ solvolysis, the enzymatic KIEs are near-intrinsic and describe a transition state that is relatively desolvated at the reaction center. The inability of CTA to catalyze NAD^+ methanolysis is also consistent with desolvation at the reaction center. Together with the observation that CTA catalyzes ADP-ribosylation with inversion of configuration at the anomeric carbon (Oppenheimer, N. J. *J. Biol. Chem.* **1978**, *253*, 4907−4910), NAD^+ hydrolysis by CTA is best described by a concerted displacement mechanism involving an enzyme-directed water nucleophile. The small, inverse solvent deuterium KIE demonstrates that a rate-limiting proton transfer does not characterize the CTA reaction coordinate. Using bond-energy bond-order vibrational analysis, the KIEs for NAD^+ hydrolysis by CTA have been used to model a transition state geometry. The model is consistent with a highly dissociative, concerted mechanism, characterized by distances from the anomeric carbon to the leaving group and incoming nucleophile of approximately 2.2 and 3.3 Å, respectively. There is significant oxocarbonium ion character and hyperconjugation within the ribose ring. The γ- and δ-secondary KIEs are evidence for enzyme−substrate interactions that are remote from the reaction center and are unique to enzymatic stabilization of the transition state.

Introduction

Cholera toxin is an exotoxin of the bacteria *Vibrio cholerae* and is the causative agent of the severe diarrhea and dehydration associated with cholera fatalities. The hetero-oligomeric toxin is composed of a pentamer of B subunits (11.6 kDa each),[1] through which the toxin binds to G_{M1} gangliosides on the surface of intestinal epithelial cells,[2] and a loosely associated A subunit (27.2 kDa),[3] which enters the cytosol. The A subunit is composed of an A1 (21.8 kDa) and an A2 (5.4 kDa) polypeptide that are linked by a disulfide bond. Reduction of the disulfide bond yields the catalytically active A1 polypeptide (CTA).[4] CTA, possibly in association with an ADP-ribosylation factor,[5] uses NAD^+ (oxidized nicotinamide adenine dinucleotide) as a substrate, cleaves the N-glycosidic bond to nicotinamide, and transfers the ADP-ribose to a specific Arg in $G_{s\alpha}$. $G_{s\alpha}$ is a GTP-binding protein that regulates adenylate cyclase. The intrinsic GTPase activity of ADP-ribosylated $G_{s\alpha}$ is inhibited,[6] leading to stimulation of adenylate cyclase, high concentrations of intracellular cAMP, and the net efflux of ions and water into the lumen of the small intestine.[7] Comparison of the primary structure of cholera toxin with that of *Escherichia coli* heat-labile enterotoxin reveals approximately 80% identity.[8] While biosynthetic processing of these toxins differ, they are catalytically indistinguishable.[9] Cholera toxin and *E. coli* heat-labile enterotoxin are members of a family of ADP-ribosylating toxins which also includes diphtheria toxin, *Pseudomonas aeruginosa* exotoxin A, and pertussis toxin.[10]

* Address correspondence to: V. L. Schramm, Department of Biochemistry, Albert Einstein College of Medicine, 1300 Morris Park Avenue, Bronx, NY 10461; phone (718) 430-2813; fax (718) 430-8565; e-mail vern@aecom.yu.edu.

⊗ Abstract published in *Advance ACS Abstracts,* December 15, 1996.

(1) Zhang, R.-G.; Westbrook, M. L.; Westbrook, E. M.; Scott, D. L.; Otwinowski, Z.; Maulik, P. R.; Reed, R. A.; Shipley, G. G. *J. Mol. Biol.* **1995**, *251*, 550−562.

(2) Merritt, E. A.; Sarfaty, S.; Van Den Akker, F.; L'Hoir, C.; Martial, J. A.; Hol, W. G. J. *Protein Sci.* **1994**, *3*, 166−175.

(3) Zhang, R.-G.; Scott, D. L.; Westbrook, M. L.; Nance, S.; Spangler, B. D.; Shipley, G. G.; Westbrook, E. M. *J. Mol. Biol.* **1995**, *251*, 563−573.

(4) Mekalanos, J. J.; Collier, R. J.; Romig, W. R. *J. Biol. Chem.* **1979**, *254*, 5855−5861.

(5) For a review, see: Welsh, C. F.; Moss, J.; Vaughan, M. In *Bacterial Toxins and Virulence Factors in Disease, Handbook of Natural Toxins*; Moss, J., Iglewski, B., Vaughan, M., Tu, A. T., Eds.; Marcel Dekker, Inc.: New York, 1995; Vol. 8, pp 257−280.

(6) (a) Cassel, D.; Selinger, Z. *Proc. Natl. Acad. Sci. U.S.A.* **1977**, *74*, 3307−3311. (b) Cassel, D.; Eckstein, F.; Lowe, M.; Selinger, Z. *J. Biol. Chem.* **1979**, *254*, 9835−9838. (c) Freissmuth, M.; Gilman, A. G. *J. Biol. Chem.* **1989**, *264*, 21907−21914.

(7) (a) Field, M. In *Physiology of the Gastrointestinal Tract*; Johnson, L. R., Ed.; Raven Press: New York, 1981; pp 963−982. (b) Field, M.; Rao, M. C.; Chang, E. B. *N. Engl. J. Med.* **1989**, *321*, 800−806. (c) Field, M.; Rao, M. C.; Chang, E. B. *N. Engl. J. Med.* **1989**, *321*, 879−883.

(8) (a) Dallas, W. S.; Falkow, S. *Nature* **1980**, *288*, 499−501. (b) Yamamoto, T.; Gojobori, T.; Yokota, T. *J. Bacteriol.* **1987**, *169*, 1352−1357. (c) Yamamoto, T.; Nakazawa, T.; Miyata, T.; Kaji, A.; Yokota, T. *FEBS Lett.* **1984**, *169*, 241−246.

(9) For a review, see: Holmes, R. K.; Jobling, M. G.; Connell, T. D. In *Bacterial Toxins and Virulence Factors in Disease, Handbook of Natural Toxins*; Moss, J., Iglewski, B., Vaughan, M., Tu, A. T., Eds.; Marcel Dekker, Inc.: New York, 1995; Vol. 8, pp 225−255.

(10) For a review, see: Domenighini, M.; Pizza, M.; Rappuoli, R. In *Bacterial Toxins and Virulence Factors in Disease, Handbook of Natural Toxins*; Moss, J., Iglewski, B., Vaughan, M., Tu, A. T., Eds.; Marcel Dekker, Inc.: New York, 1995; Vol. 8, pp 59−80.

S0002-7863(96)02191-9 CCC: $14.00

In vitro, CTA catalyzes the ADP-ribosylation of simple guanidino compounds, including arginine, guanidine, agmatine, arginine methyl ester, *N*-guanyltyramine, and several guanylhydrazones.[11−15] The kinetic mechanism for ADP-ribosyl transfer by CTA is apparently random sequential and has been reported to be characterized by rapid equilibrium binding and dissociation of substrates.[13,15] In the absence of an appropriate guanidino compound, CTA also catalyzes the slow hydrolysis of NAD^+ [16−18] to form ADP-ribose and nicotinamide. NAD^+ hydrolysis by CTA is an irreversible reaction with a ΔG comparable to that for hydrolysis of the γ-phosphate of ATP.[19] The transition state structure for the NAD^+ glycohydrolase activity of CTA, based on kinetic isotope effect studies, is reported here.

Endogenous NAD^+ glycohydrolases are ubiquitously distributed in procaryotes and eucaryotes. In addition to NAD^+ hydrolysis, NAD^+ glycohydrolases from calf spleen, porcine brain, and *Bungarus fasciatus* venom, for example, catalyze transglycosidation and NAD^+ alcoholysis through a mechanism characterized by a stabilized enzyme−ADP-ribose intermediate.[20−24] These reactions occur with retention of configuration at the anomeric carbon.[22,25] In contrast, microbial NAD^+ glycohydrolases, including those from *Bacillus subtilis* and *Neurospora crassa*, as well as CTA from *V. cholerae*, do not catalyze transglycosidation or NAD^+ alcoholysis.[26,27] ADP-ribosyl transfer by CTA occurs with inversion of configuration at the anomeric carbon.[26]

In spite of these mechanistic dissimilarities, both enzymatic and nonenzymatic NAD^+ hydrolysis have been shown to be generally characterized by a dissociative, electropositive transition state. The α-secondary ^2H kinetic isotope effects (KIEs) for nonenzymatic NR^+ (nicotinamide riboside), NMN^+ (nicotinamide mononucleotide),and NAD^+ hydrolysis range from 1.101 to 1.151, depending on pH.[28,29] Formation of a ribose diol anion has been proposed to explain the observation that base-catalyzed NAD^+ hydrolysis is dissociative.[30] In addition, the α-secondary ^2H KIEs for NMN^+ hydrolysis by *N. crassa* and porcine brain NAD^+ glycohydrolases are 1.100 and 1.132, respectively.[28] The electropositive character of the transition state for nonenzymatic and calf spleen NAD^+ glycohydrolase-catalyzed hydrolysis of pyridinium analogs of NAD^+ is shown by β_{lg} values of −1.11 and −0.90, respectively.[31]

To further elucidate the mechanism of dissociative NAD^+ hydrolysis, this study has undertaken the first complete characterization of a transition state structure for the enzymatic hydrolysis of NAD^+, as catalyzed by CTA. A transition state structure provides unique information about the substrate at the transition state of a reaction, when binding to the enzyme is tighter than at any other point on the reaction coordinate.[32] The transition state has been characterized through multiple V/K KIEs and through comparison with KIEs measured in parallel for pH-independent NAD^+ solvolysis. The transition state geometry has been modeled using bond-energy bond-order vibrational analysis (BEBOVIB), and a model describing the possible origin of the catalytic power of CTA is presented. A transition state geometry can serve as the basis for transition state structure-based inhibitor design, with the potential result of therapeutically useful inhibitors of cholera toxin.[33−35]

Materials and Methods

Enzymes. Cholera toxin A protomer was purchased as a lyophilized powder from List Biological Laboratories, Inc., and was provided free of contamination from B subunits or intact toxin according to nondenaturing polyacrylamide gel electrophoresis. The A protomer was resuspended as recommended by the supplier and used at concentrations of 75−160 μg/mL (2.8−5.9 μM). Unless specified otherwise, activity was assayed at 37 °C in 200 mM potassium phosphate, pH 7.0, 20 mM DTT (dithiothreitol), and 6 mM NAD^+. The A protomer was preactivated in buffer and DTT for 20 min at 37 °C to allow for reduction of the catalytic A1 polypeptide (CTA) away from A2.[4,16]

NAD^+ glycohydrolase (EC 3.2.2.5), partially purified from *N. crassa* crude extract, was purchased from Sigma. The preparation was further purified to remove a nucleotide pyrophosphatase activity. All purification steps were performed at 4 °C. Approximately 50 units of the crude NAD^+ glycohydrolase was dialyzed against 15 mM potassium phosphate, pH 7.0, and applied to a Pharmacia MonoQ HR 10/10 column. The column was washed with 20 mL equilibration buffer followed by an 80 mL gradient to 1 M KCl in the same buffer. The contaminating nucleotide pyrophosphatase activity eluted in a sharp peak at approximately 0.5 M KCl. NAD^+ glycohydrolase activity eluted in a broad peak over much of the KCl gradient. Fractions containing NAD^+ glycohydrolase activity in the absence of nucleotide pyrophosphatase activity were pooled and concentrated to about 1.3 mL in an Amicon Centriprep-10, frozen on dry ice in aliquots of approximately 0.02 units each, and stored at −70 °C. NAD^+ glycohydrolase prepared and stored in this manner maintains catalytic activity for at least 12 months.

Measurement of Kinetic Constants. Initial rate data for NAD^+ hydrolysis were obtained according to the method of Moss and coworkers,[13,16] with minor modifications. Initial rate assays (270 μL) included 0.5−1 μCi [(4-^3H)nicotinamide]NAD^+ (Amersham, 1.0−2.4 Ci/mmol) along with 1−32 mM unlabeled NAD^+. Aliquots (50 μL) were removed from each reaction at 20−30 min intervals and applied

(11) Moss, J.; Vaughan, M. *J. Biol. Chem.* **1977**, *252*, 2455−2457.
(12) Mekalanos, J. J.; Collier, R. J.; Romig, W. R. *J. Biol. Chem.* **1979**, *254*, 5849−5854.
(13) Osborne, J. C., Jr.; Stanley, S. J.; Moss, J. *Biochemistry* **1985**, *24*, 5235−5240.
(14) (a)Soman, G.; Miller, J. F.; Graves, D. J. *Methods Enzymol.* **1984**, *106*, 403−410. (b) Soman, G.; Narayanan, J.; Martin, B. L.; Graves, D. J. *Biochemistry* **1986**, *25*, 4113−4119.
(15) Larew, J. S.-A.; Peterson, J. E.; Graves, D. J. *J. Biol. Chem.* **1991**, *266*, 52−57.
(16) Moss, J.; Manganiello, V. C.; Vaughan, M. *Proc. Natl. Acad. Sci. U.S.A.* **1976**, *73*, 4424−4427.
(17) Moss, J.; Stanley, S. J.; Lin, M. C. *J. Biol. Chem.* **1979**, *254*, 11993−11996.
(18) Galloway, T. S.; Van Heyningen, S. V. *Biochem. J.* **1987**, *244*, 225−230.
(19) Zatman, L. J.; Kaplan, N. O.; Colowick, S. P. *J. Biol. Chem.* **1953**, *200*, 197−212.
(20) Swislocki, N. I.; Kaplan, N. O. *J. Biol. Chem.* **1967**, *242*, 1083−1088.
(21) Schuber, F.; Travo, P.; Pascal, M. *Eur. J. Biochem.* **1976**, *69*, 593−602.
(22) Oppenheimer, N. J. *FEBS Lett.* **1978**, *94*, 368−370.
(23) (a) Yost, D. A.; Anderson, B. M. *J. Biol. Chem.* **1982**, *257*, 767−772. (b) Yost, D. A.; Anderson, B. M. *J. Biol. Chem.* **1983**, *258*, 3075−3080.
(24) Tarnus, C.; Muller, H. M.; Schuber, F. *Bioorg. Chem.* **1988**, *16*, 38−51.
(25) Pascal, M.; Schuber, F. *FEBS Lett.* **1976**, *66*, 107−109.
(26) Oppenheimer, N. J. *J. Biol. Chem.* **1978**, *253*, 4907−4910.
(27) (a) Everse, J.; Everse, K. E.; Kaplan, N. O. *Arch. Biochem. Biophys.* **1975**, *169*, 702−713. (b) Everse, K. E.; Everse, J.; Simeral, L. S. *Methods Enzymol.* **1980**, *66*, 137−144 and references therein.
(28) Bull, H. G.; Ferraz, J. P.; Cordes, E. H.; Ribbi, A.; Apitz-Castro, R. *J. Biol. Chem.* **1978**, *253*, 5186−5192.
(29) Ferraz, J. P.; Bull, H. G.; Cordes, E. H. *Arch. Biochem. Biophys.* **1978**, *191*, 431−436.
(30) Johnson, R. W.; Marschner, T. M.; Oppenheimer, N. J. *J. Am. Chem. Soc.* **1988**, *110*, 2257−2263.
(31) Tarnus, C.; Schuber, F. *Bioorg. Chem.* **1987**, *15*, 31−42.
(32) Wolfenden, R. In *Transition States of Biochemical Processes*; Gandour, R. D., Schowen, R. L., Eds.; Plenum Press: New York, 1978; pp 555−578.
(33) (a) Horenstein, B. A.; Schramm, V. L. *Biochemistry* **1993**, *32*, 7089−7097. (b) Horenstein, B. A.; Schramm, V. L. *Biochemistry* **1993**, *32*, 9917−9925.
(34) Boutellier, M.; Horenstein, B. A.; Semenyaka, A.; Schramm, V. L.; Ganem, B. *Biochemistry* **1994**, *33*, 3994−4000.
(35) Schramm, V. L.; Horenstein, B. A.; Kline, P. C. *J. Biol. Chem.* **1994**, *269*, 18259−18262.

Table 1. Kinetic Isotope Effects for Cholera Toxin-Catalyzed and Nonenzymatic NAD^+ Hydrolysis

substrates	isotopic label, type of isotope effect	cholera toxin experimental KIEs[a]	nonenzymatic experimental KIEs[a,c]
$[H_N1'\text{-}^3H]NAD^+$, $[C_N5'\text{-}^{14}C]NAD^+$	$H_N1'\text{-}^3H$, α-secondary	1.186 ± 0.004 (5)	1.238 ± 0.006 (3)
$[H_N2'\text{-}^3H]NAD^+$, $[C_N5'\text{-}^{14}C]NAD^+$	$H_N2'\text{-}^3H$, β-secondary	1.108 ± 0.004 (3)	1.139 ± 0.006 (7)
$[H_N4'\text{-}^3H]NAD^+$, $[C_N5'\text{-}^{14}C]NAD^+$	$H_N4'\text{-}^3H$, γ-secondary	0.986 ± 0.003 (3)	0.996 ± 0.001 (3)
$[H_N5'\text{-}^3H]NAD^+$, $[C_N5'\text{-}^{14}C]NAD^+$	$H_N5'\text{-}^3H$, δ-secondary	1.020 ± 0.003 (4)	0.999 ± 0.004 (5)
$[H_N5'\text{-}^3H]NAD^+$, $[C_A8\text{-}^{14}C]NAD^+$	$H_N5'\text{-}^3H$, δ-secondary	1.019 ± 0.002 (3)	1.000 ± 0.006 (5)
$[C_N1'\text{-}^{14}C]NAD^+$, $[H_N5'\text{-}^3H]NAD^+$	$C_N1'\text{-}^{14}C$, primary	1.030 ± 0.005 (3)[b]	1.019 ± 0.004 (8)
$[N_N1\text{-}^{15}N,C_N5'\text{-}^{14}C]NAD^+$, $[H_N5'\text{-}^3H]NAD^+$	$N_N1\text{-}^{15}N$, primary	1.029 ± 0.004 (4)[b]	1.024 ± 0.011 (8)
$[N_N1\text{-}^{15}N,C_N1'\text{-}^{14}C]NAD^+$, $[H_N5'\text{-}^3H]NAD^+$	$N_N1\text{-}^{15}N$, $C_N1'\text{-}^{14}C$, primary double	1.052 ± 0.004 (3)[b]	1.041 ± 0.004 (6)

[a] The number in parenthesis is the number of KIE experiments. For each experiment, the value for the KIE was measured in quadruplicate. The KIE values for all experiments were averaged, and the standard deviation between experiments was calculated. [b] KIEs obtained using $[H_N5'\text{-}^3H]NAD^+$ as the remote-labeled substrate were corrected for the $H_N5'\text{-}^3H$ KIE according to the expression KIE × $(H_N5'\text{-}^3H)$KIE. [c] KIEs measured for NAD^+ solvolysis were corrected for the temperature difference between enzymatic (37 °C) and nonenzymatic (100 °C) reactions according to the equation $\ln({}^Dk_2) = (T_1/T_2)\ln({}^Dk_1)$ as described in the text.

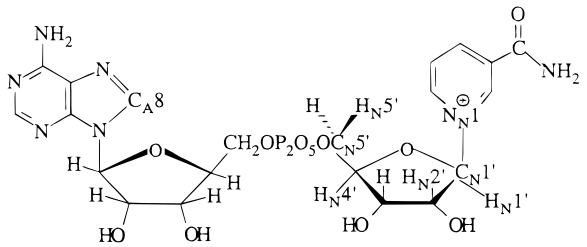

Figure 1. Structure of NAD^+ indicating the numbering of atoms in the molecule where radioactive or heavy-atom isotopes are incorporated. Subscripts N and A indicate the NMN^+ and AMP portions of the molecule, respectively. Primed numbers indicate atomic locations in the ribosyl portions of the molecule.

to 1 mL Bio-Rad Dowex AG1-X2 columns, washed and equilibrated in H_2O. Two 2.5 mL fractions were collected from each column in H_2O and were supplemented with 18 mL of Liquiscint (National Diagnostics). Approximately 97% of labeled nicotinamide is recovered while labeled NAD^+ does not elute. Kinetic constants were calculated from the fit of the initial velocity data to the Michaelis−Menten equation, using Kaleidagraph (version 2.1).

Isotopically Labeled NAD^+. Isotopically labeled NAD^+ was prepared enzymatically from appropriately labeled glucose, ribose 5-phosphate, ATP, and/or nicotinic acid.[36] The isotopically labeled substrates prepared for this study are listed in Table 1, and the nomenclature is diagramed in Figure 1.

Measurement and Calculation of KIEs. The V/K KIEs were measured using the competitive-radiolabel method.[37,38] Along with carrier substrate, reaction mixtures contained trace amounts of two types of radioactively-labeled NAD^+, each containing a distinct isotopic label. One type of labeled NAD^+ contained a radioactive isotope (^3H, for example) at an isotopically-sensitive position, which is a position expected to experience changes in bond order during the conversion of the ground state to the transition state. The other type of labeled NAD^+ contained a radioactive isotope (^{14}C, for example) at an isotopically-insensitive position, but a natural-abundance isotope in the position corresponding to that labeled in the NAD^+ described above.

The relative rates of hydrolysis of these two types of labeled NAD^+ were measured by determining the ratio of the radioactive isotopes in the product. The NAD^+ containing ^{14}C at an isotopically-insensitive position is expected to be hydrolyzed at the same rate as NAD^+ containing natural-abundance isotopes at every position. However, the NAD^+ containing ^3H at an isotopically-sensitive position is expected to be hydrolyzed at a rate reflecting the ^3H KIE at that position. In this way, the rate of hydrolysis of NAD^+ containing a heavy isotope at an isotopically-sensitive position is compared with that of NAD^+ containing a natural-abundance isotope at the same position. The remote label (^{14}C in this example) serves only to provide a radioactive probe for the rate of hydrolysis of unlabeled NAD^+.

Measurement of ^{15}N KIEs required a variation of this procedure. Since ^{15}N is not a radioactive isotope, ^{15}N-labeled NAD^+ contained an additional, radioactive label (^{14}C) within the same molecule. The ^{14}C was used in both isotopically-sensitive and insensitive positions, depending on the type of KIE being measured. The rate of hydrolysis of ^{15}N-labeled NAD^+ was compared to that of NAD^+ containing ^3H in a remote position. All combinations of substrates used in KIE measurements are listed in Table 1.

Each 250 μL reaction mixture used in a KIE measurement contained $(3-6) \times 10^5$ cpm (counts per minute) labeled NAD^+, along with 6 mM carrier NAD^+. Labeled NAD^+ was repurified prior to use to remove any ADP-ribose generated during storage. The required ^3H- and ^{14}C-labeled NAD^+ species were combined, dried under vacuum, resuspended in 50 μL of 6 mM carrier NAD^+, and applied to a 1 mL DEAE (diethylaminoethyl) Sephadex A25-acetate column, equilibrated in 0.1 M ammonium acetate, pH 5.0. NAD^+ was eluted in 6 mL of equilibration buffer while ADP-ribose remained bound to the column. The labeled NAD^+ was freeze-dried, resuspended in 1 mL of 50% ethanol, and dried under vacuum to remove residual ammonium acetate. All NAD^+ preparations used in KIE measurements were >99% NAD^+.

For each KIE measurement, two parallel reactions containing identical substrate mixtures were analyzed for the isotopic ratio in the product, ADP-ribose. Reaction progress was monitored by C_{18} reverse phase HPLC in 50 mM ammonium acetate, pH 5.0. Purified *N. crassa* NAD^+ glycohydrolase was used in one reaction to obtain 100% NAD^+ hydrolysis. CTA was used in the parallel reaction to achieve partial (20−35%) NAD^+ hydrolysis. The ADP-ribose purified from the complete reaction provides the control isotopic ratio. The isotopic ratio in ADP-ribose isolated from the partial reaction is influenced by the expression of a KIE. ADP-ribose was purified from quadruplicate aliquots (50 μL each) from both the partial and complete reactions. Aliquots were applied to 1 mL DEAE Sephadex A25-acetate columns (8 total) equilibrated in 20 mM ammonium bicarbonate, pH 8.0. Nicotinamide and NAD^+ were eluted in 6 mL of 150 mM ammonium bicarbonate, pH 8.0, followed by elution and collection of ADP-ribose in 10 fractions of 0.5 mL at 800 mM ammonium bicarbonate, pH 8.0. H_2O (0.5 mL) was added to each fraction, followed by 9 mL of Liquiscint.

By liquid scintillation counting of ADP-ribose, the ratio of radioactivity in the remote position to that in the isotopically-sensitive position was measured. For each complete data set, the average isotopic ratio in ADP-ribose isolated from the partial NAD^+ hydrolysis reaction, and from the 100% NAD^+ hydrolysis reaction, was calculated. The ratio of these values is the observed KIE (KIE_{obsd}) and is a function of both the isotope effect and the fraction of conversion of substrates to products (f). The value for KIE_{obsd} is corrected for f according to the following equation:

$$\text{corrected KIE} = \ln(1 - \text{KIE}_{\text{obsd}}\, f)/\ln(1 - f)$$

Dual-channel ^3H and ^{14}C counting was continued until a T-test (99.999% confidence interval) left at least 6 counting cycles for which the standard deviation was less than 1.0% from the average of the

(36) Rising, K. A.; Schramm, V. L. *J. Am. Chem. Soc.* **1994**, *116*, 6531−6536.

(37) (a) Dahlquist, F. W.; Rand-Meir, T.; Raftery, M. A. *Proc. Natl. Acad. Sci. U.S.A.* **1968**, *61*, 1194−1198. (b) Dahlquist, F. W.; Rand-Meir, T.; Raftery, M. A. *Biochemistry* **1969**, *8*, 4214−4221.

(38) Parkin, D. W. In *Enzyme Mechanism from Isotope Effects*; Cook, P. F., Ed.; CRC Press: Boca Raton, FL, 1991; pp 269−290.

corrected KIEs. For most experiments, this statistical analysis provided 10−20 counting cycles having a standard deviation of less that 0.6% from the average.

The value for *f* in the CTA reaction was derived both by dividing the average cpm in ADP-ribose into the total cpm applied to a column and by collecting and quantitating unreacted NAD^+ from one column. The two methods yielded equivalent results. This latter procedure was also used for each NAD^+ glycohydrolase reaction, and the cpm eluting as ADP-ribose was consistently >99% of the cpm applied to the column.

[H_N5'-^{3}H]NAD^+ was used as the remote-labeled substrate for measurement of the primary ^{14}C, the primary ^{15}N, and the primary double KIEs. However, a significant KIE was observed with [H_N5'-^{3}H]NAD^+, using [C_N5'-^{14}C]NAD^+ as the remote-labeled substrate. This result required that the primary KIEs be corrected for the value of the H_N5'-^{3}H KIE. Thus, all KIEs were normalized according to a C_N5'-^{14}C KIE of unity. The value of unity for the C_N5'-^{14}C-KIE was confirmed by the observation of equivalent H_N5'-^{3}H KIEs using either [C_N5'-^{14}C]- or [C_A8-^{14}C]NAD^+ as the remote-labeled substrate (see Table 1).

A family of KIEs for nonenzymatic NAD^+ hydrolysis was measured as described above, except that partial NAD^+ hydrolysis was obtained by boiling (100 °C) for 7 min in 50 mM sodium acetate, pH 4.0, followed by freezing on dry ice. Under these conditions, nonenzymatic NAD^+ hydrolysis is pH-independent and water-catalyzed[30] and no extraneous side products are produced. The KIEs measured in solution were corrected for the temperature difference between the enzymatic and nonenzymatic reactions (37 versus 100 °C, respectively) in order to allow comparison of the two families of KIEs. The nonenzymatic KIEs were corrected according to the equation

$$\ln({}^{D}k_2) = (T_1/T_2)\ln({}^{D}k_1)$$

where T_1 is the temperature used for nonenzymatic NAD^+ hydrolysis (373.15 K), T_2 is that used for CTA-catalyzed NAD^+ hydrolysis (310.15 K), ${}^{D}k_1$ is the KIE observed in solution (a deuterium KIE in this example), and ${}^{D}k_2$ is the corrected KIE.

Solvent Deuterium KIE. A direct comparison of initial rates in H_2O and D_2O was made using reactions of 270 μL, in duplicate or triplicate for each solvent, containing 200 mM potassium phosphate, pH/pD 7.0, 20 mM DTT, 6 mM NAD^+, 0.5 μCi [(4-^{3}H)nicotinamide]-NAD^+ and 75 μg/mL CTA. The reactions were prepared by first aliquoting and freeze-drying a mixture of CTA and DTT and a mixture of NAD^+ and ^{3}H-NAD^+. The CTA/DTT samples were reconstituted in potassium phosphate, pH/pD 7.0, and the CTA was preactivated as described. The substrate samples were resuspended in H_2O/D_2O and added to the enzyme. Initial rates were measured as described above.

NAD^+ Methanolysis. Methyl-ADP-ribose was prepared by boiling 6 mM NAD^+ in 6 M methanol, 50 mM sodium acetate, pH 4.1, for 7 min. The retention time of methyl-ADP-ribose was determined by C_{18} reverse phase HPLC in 50 mM ammonium acetate, pH 5.0. At a flow rate of 2 mL/min, methyl-ADP-ribose elutes at 3.5 min while ADP-ribose, nicotinamide, and NAD^+ elute at 2.5, 5.2, and 6.5 min, respectively. The peak at 3.5 min was not observed in a parallel experiment in which methanol was omitted. On 1 mL DEAE Sephadex A25-acetate columns, equilibrated in 20 mM ammonium bicarbonate, pH 8.0, CH_3OH elutes in 8 mL of equilibration buffer, while elution of methyl-ADP-ribose requires 10 mL of 800 mM ammonium bicarbonate, pH 8.0.

Each 120 μL enzymatic reaction used to investigate methanolysis contained 200 mM potassium phosphate, pH 7.0, 20 mM DTT, 6 mM NAD^+, and 100 μg/mL CTA. Methanol was included in each reaction as 2 μCi $^{14}CH_3OH$ with sufficient carrier to yield final CH_3OH concentrations in the range of 1−5 M (4−20%). Control reactions minus CTA were done at each CH_3OH concentration. Reactions were incubated for 5 h at 37 °C and were analyzed by HPLC and by anion exchange chromatography. Fractions from anion exchange columns were analyzed for unreacted $^{14}CH_3OH$ and for ^{14}C-methyl-ADP-ribose by liquid scintillation counting.

Transition State Modeling. Transition state geometries were modeled using the bond-energy bond-order vibrational analysis approach as implemented in the program BEBOVIB-IV (Quantum Chemistry Program Exchange, No. 337)[39] and as previously described.[40−42]

Bond lengths and angles for reactant state NAD^+ were derived from the crystal structure of the lithium salt of NAD^+ dihydrate.[43] The structure was reduced to NMN^+ with all hydrogens included. A structural energy minimization calculation was performed for the complete NMN^+ structure using the PM3 semiempirical method and the PRECISE option, as implemented in MOPAC 6.0. Two dihedral angles in the ribose ring were frozen during the minimization to maintain the ribosyl 3′-endo conformation. The final reactant structure used for BEBOVIB calculations included all atoms at least two bonds from each labeled, isotopically-sensitive position. The model included a closed, 3′-endo, ribosyl ring lacking the 3′-OH, 3′-H, and all other hydroxylic hydrogens. The nicotinamide ring was not closed and included only the endocyclic nitrogen, C_N2, C_N3, C_N5, C_N6, and the hydrogens on C_N2 and C_N6. The validity of using such a cutoff model is discussed by Sims and Lewis.[44] The reactant state model, diagramed in Figure 2a, was characterized by a $N_N1-C_N1'-C_N2'-H_N2'$ dihedral angle of 35°.

The starting structure for the ribose ring portion of the transition state was derived from the crystal structure of ribonolactone.[45] A hydrogen atom was substituted for the carbonyl oxygen on C1. Bond lengths and angles were obtained from a structural energy minimization using MOPAC, as described above. Two dihedral angles, corresponding to those frozen during the reactant state minimization, were also constrained in this calculation to maintain the ribosyl 3′-exo conformation. The cutoff model defining the nicotinamide ring in the reactant state structure was incorporated into the transition state model at the same $O_N4'-C_N1'-N_N1-C_N6$ dihedral angle of 28°, along with an oxygen atom as a model of the incoming water nucleophile. The oxygen atom was placed at a 180° angle with respect to the cleaving N-glycosidic bond, and both breaking and forming bonds were modeled orthogonal to the plane defined by the atoms attached to the anomeric carbon. The starting transition state model was characterized by a $N_N1-C_N1'-C_N2'-H_N2'$ dihedral angle of 0.6°.

Force constants for bond stretching, angle bending, and torsional bending were from reported values[44,46,47] and are listed in the Supporting Information. The reaction coordinate was modeled by coupling the bond stretching of the $C_N1'-N_N1$ and $C_N1'-O$ bonds, using a coupling constant of 1.1. Inversion of configuration at the anomeric carbon was modeled by including coupling constants between the stretching modes of $C_N1'-N_N1$ and $C_N1'-O$ and the angle bending modes defined by $N_N1-C_N1'-O_N4'$, $N_N1-C_N1'-C_N2'$, $N_N1-C_N1'-H_N1'$, $O-C_N1'-O_N4'$, $O-C_N1'-C_N2'$, and $O-C_N1'-H_N1'$ (coupling constant is +0.05 or −0.05 depending on whether the angle does or does not include the bond to which it is coupled, respectively).

Transition state structure space was searched by varying bond orders (*n*) to the leaving group and the incoming nucleophile and by adjusting other bond orders within the molecule in a concerted manner. Bond orders to the leaving group and nucleophile were input parameters. Subtracting the sum of these bond orders from the reactant state N-glycosidic bond order gave the amount of bond order lost from the anomeric carbon at the transition state. The loss of bond order at the anomeric carbon was compensated by adjusting the $C_N1'-O_N4'$, $C_N1'-C_N2'$, and $C_N2'-H_N2'$ bond orders according to equations 1−3, with a ground state N-glycosidic bond order of 0.902. In these expressions, *f*(deloc) is the proportion of the bond order lost at the anomeric carbon

(39) Sims, L. B.; Burton, G. W.; Lewis, D. E. *Quantum Chemistry Program Exchange, No. 337*; Indiana University: Bloomington, IN, 1977.
(40) Mentch, F.; Parkin, D. W.; Schramm, V. L. *Biochemistry* **1987**, *26*, 921−930.
(41) Parkin, D. W.; Mentch, F.; Banks, G. A.; Horenstein, B. A.; Schramm, V. L. *Biochemistry* **1991**, *30*, 4886−4594.
(42) Horenstein, B. A.; Parkin, D. W.; Estupiñán, B.; Schramm, V. L. *Biochemistry* **1991**, *30*, 10788−10795.
(43) Reddy, B. S.; Saenger, W.; Mühlegger, K.; Weimann, G. *J. Am. Chem. Soc.* **1981**, *103*, 907−914.
(44) Sims, L. B.; Lewis, D. E. *Isot. Org. Chem.* **1984**, *6*, 161−259.
(45) Kinoshita, Y.; Ruble, J. R.; Jeffrey, G. A. *Carbohydr. Res.* **1981**, *92*, 1−7.
(46) Wilson, E. B.; Decius, J. C.; Cross, P. C. *Molecular Vibrations*; McGraw-Hill Book Co., Inc.: New York, 1955.
(47) Sims, L. B.; Fry, A. *Special Publication No. 1*; University of Arkansas: Fayetteville, AR, 1974.

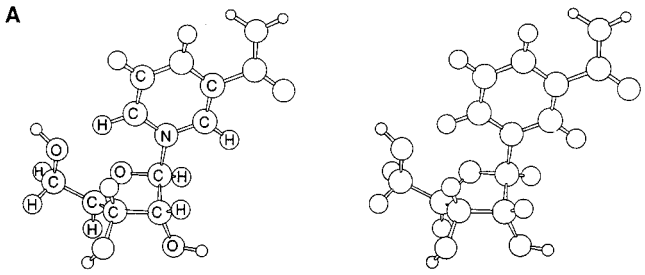

Reactant State Bond Orders and Bond Lengths

Bond	Bond Length (Å)	Bond Order
C_N1'-N_N1	1.523	0.902
C_N1'-O_N4'	1.416	1.100
C_N1'-C_N2'	1.572	0.810
C_N1'-H_N1'	1.116	0.948
C_N2'-H_N2'	1.111	0.963

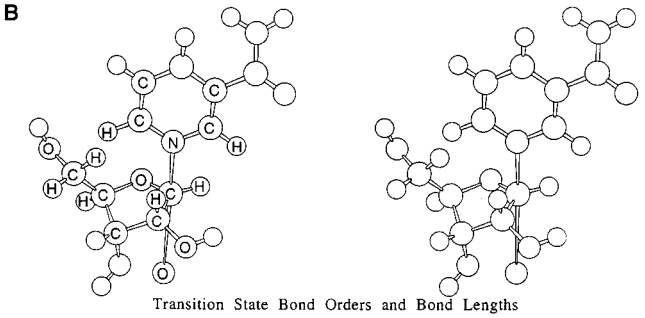

Transition State Bond Orders and Bond Lengths

Bond	Bond Length (Å)	Bond Order
C_N1'-N_N1	2.162	0.107
C_N1'-O_N4'	1.220	2.115
C_N1'-C_N2'	1.552	0.866
C_N1'-H_N1'	1.111	0.963
C_N2'-H_N2'	1.129	0.907
C_N1'-O	3.309	0.002

Figure 2. Stereoviews, bond lengths, and bond orders of the ground state NAD^+ model and the transition state model for NAD^+ hydrolysis by CTA. Panel A shows the structure, bond lengths, and bond orders of ground state NR^+, with atom labels indicating atoms included in the cutoff model used in BEBOVIB calculations. NAD^+ coordinates,[43] and a MOPAC all-atom structural energy minimization, were used to construct the model. The reactant model has a $O_N4'-C_N4'-C_N5'$ bond angle of 107°. Panel B shows the structure, bond lengths, and bond orders of the transition state model for NAD^+ hydrolysis by CTA, calculated at a value for *f*(deloc) of 1.35. Ribonolactone coordinates,[45] and a MOPAC all-atom structural energy minimization, were used to construct the starting transition state model. The major features of the model include minimal nucleophilic participation and substantially decreased bond order between the anomeric carbon and nicotinamide. C_N1' has rehybridized to become sp^2-like and the $C_N1'-O_N4'$ bond has essentially double-bond character. The ribose has a 3′-exo conformation, compared to a 3′-endo conformation in the reactant state, and the $C_N2'-H_N2'$ bond is nearly eclipsed with the cleaving N-glycosidic bond. The increase in the $O_N4'-C_N4'-C_N5'$ bond angle, to 128°, represents a distortion that may account for the remote γ- and δ-secondary KIEs.

that is delocalized into the ribosyl moiety and $p(C_N1'-O_N4')$ and $p(C_N1'-C_N2')$ are the proportions of this bond order assigned to each of these two bonds.

$$n(C_N1'-O_N4')^{\ddagger} = n(C_N1'-O_N4') + [0.902 - n(C_N1'-N_N1)^{\ddagger} - n(C_N1'-O)^{\ddagger}]f(\text{deloc})p(C_N1'-O_N4') \quad (1)$$

$$n(C_N1'-C_N2')^{\ddagger} = n(C_N1'-C_N2') + [0.902 - n(C_N1'-N_N1)^{\ddagger} - n(C_N1'-O)^{\ddagger}]f(\text{deloc})p(C_N1'-C_N2') \quad (2)$$

$$n(C_N2'-H_N2')^{\ddagger} = n(C_N2'-H_N2') - [n(C_N1'-C_N2')^{\ddagger} - n(C_N1'-C_N2')] \quad (3)$$

The value for $n(C_N1'-H_N1')$ was not varied in concert with the other bond orders incorporated into the model described above. The H_N1'-^3H KIE arises primarily from changes in out-of-plane bending vibrational freedom instead of from significant changes in bond stretching and bond order.[48,49] Out-of-plane bending vibrational freedom of the $C_N1'-H_N1'$ bond is defined by the assumption of sp^2-like hybridization at C_N1'. Minor adjustments of the $C_N1'-H_N1'$ bond order, following the modeling of all other KIEs, were sufficient to fit the H_N1'-^3H KIE.

Remote γ- and δ-secondary KIEs, if expressed on the enzyme, presumably arise from enzymatic distortion of the substrate at positions remote from the reaction center. Unlike KIEs measured at the reaction center, KIEs of this type cannot be described easily in terms of bond orders for the reacting bonds. Instead, remote KIEs can be modeled by incorporating various possible distortions into the transition state model and observing the effects on the calculated KIEs.

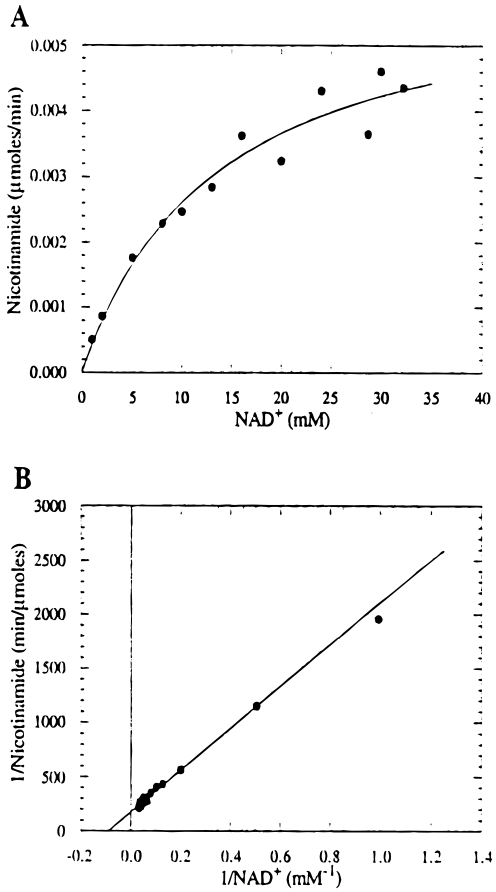

Figure 3. Michaelis−Menten plot (Panel a) and Lineweaver−Burk transformation (Panel B) of initial velocity data for CTA-catalyzed NAD^+ hydrolysis. Initial rates were measured by monitoring [4-^3H]-nicotinamide production, as described in Materials and Methods. All reactions included preactivated CTA (75 μg/mL), 200 mM potassium phosphate, pH 7.0, 20 mM DTT, and 0.5−1 μCi [(4-^3H)nicotinamide]-NAD^+. Initial velocities were analyzed using Enzfitter, and the data were fit to the Michaelis−Menten and Lineweaver−Burk equations using Kaleidagraph.

Results

Kinetic Constants. A K_m for NAD^+ of 13.5 ± 3.2 mM and a k_{cat} of 8.2 ± 0.8 min^{-1} (k_{cat}/K_m = 600 M^{-1} min^{-1}) were measured for NAD^+ hydrolysis by CTA (Figure 3). The K_m of approximately 14 mM is larger than that of 1.1−5.6 mM frequently reported in the literature.[12,13,15−18,50] This discrepancy

(48) (a) Hogg, J. L. In *Transition States of Biochemical Processes*; Gandour, R. D., Schowen, R. L., Eds.; Plenum Press: New York, 1978; pp 201−224. (b) Poirier, R. A.; Wang, Y.; Westaway, K. C. *J. Am. Chem. Soc.* **1994**, *116*, 2526−2533.

(49) Streitwieser, A., Jr.; Jagow, R. H.; Fahey, R. C.; Suzuki, S. *J. Am. Chem. Soc.* **1958**, *80*, 2326−2332.

(50) Loesberg, C.; van Rooij, H.; Smets, L. A. *Biochim. Biophys. Acta* **1990**, *1037*, 92−99.

may result from differences in assay conditions. The activity of CTA varies widely in different buffers, and CTA is activated by potassium phosphate.[16,17,51] The k_{cat} of 8 min^{-1} ($k_{cat} \approx 0.13$ s^{-1}) corresponds to that reported by Galloway and Van Heyningen.[18] Thus, CTA has a specific activity of approximately 0.3 μmol of NAD^+/min per milligram of total protein under the described assay conditions.

Comparison of Solvolytic and Enzymatic KIEs. The KIEs obtained for NAD^+ hydrolysis by CTA are summarized in Table 1. Quantitative information about transition state structures can only be obtained from intrinsic or near-intrinsic KIE values. The K_m of approximately 14 mM for NAD^+ indicates weak binding to CTA. Consideration of this with the slow hydrolytic rate of 0.13 s^{-1} indicates that a 10% commitment to catalysis for bound NAD^+ would require a second-order rate constant of 90 M^{-1} s^{-1} for E·NAD^+ formation. This value is approximately 10^{-7} of that normally found for enzyme (E)−substrate interactions and makes forward commitment unlikely.

The KIEs measured for pH-independent, water-catalyzed NAD^+ hydrolysis are also summarized in Table 1. The α-secondary ^{3}H KIE for NAD^+ solvolysis, at 1.238, is comparable to the α-secondary ^{2}H KIEs previously measured for pH-independent NMN^+ and NR^+ hydrolysis. When corrected to the ^{3}H values according to the Swain−Schaad relationship,[52] these latter KIEs are in the range of 1.15−1.21.[28,29]

A comparison of the family of KIEs for CTA-catalyzed NAD^+ hydrolysis with that for pH-independent NAD^+ solvolysis also suggests that the enzymatic KIEs have near-intrinsic values and that CTA catalysis proceeds through a single transition state characterized by rate-limiting cleavage of the N-glycosidic bond. Considering the family of enzymatic KIEs alone, the large values for these KIEs indicate that the chemistry of N-glycosidic bond cleavage is the most rate-determining step in CTA-catalyzed NAD^+ hydrolysis. The enzymatic KIEs are comparable in magnitude to those observed in solution. In particular, the α- and β-secondary KIEs are somewhat reduced on the enzyme, compared to those observed in solution, while the primary KIEs, as well as the γ- and δ-secondary KIEs, are larger in absolute magnitude for the enzyme-catalyzed reaction. Nonenzymatic KIEs are representative of solution chemistry, which is often characterized by (but is not limited to) a single rate-limiting transition state. The similarity between the enzymatic and nonenzymatic KIEs suggests that both reactions express intrinsic or near-intrinsic KIEs and that both pass through a single rate-limiting transition state. It is improbable that both reactions proceed through the same set of multiple, partially rate-limiting transition states that have similar relative energies. Also, the primary double KIE observed on CTA (1.052 ± 0.004) equals (within error) the product of the individual primary ^{14}C and ^{15}N KIEs (1.060 ± 0.006). This result is consistent with the absence of a significant forward commitment factor prior to the first irreversible step in the reaction coordinate. The value of the primary double KIE is not an ideal test for this reaction coordinate characteristic when both of the primary KIEs are small, as observed in this system.

Further evidence regarding the mechanism of N-glycosidic bond cleavage is derived from the small solvent deuterium KIE on V/K, 0.82 ± 0.09 (five experiments), which indicates that NAD^+ hydrolysis by CTA is not characterized by a rate-limiting proton transfer. Thus, the first irreversible step in the CTA reaction coordinate is likely to be uniquely identified with the rate-limiting cleavage of the N-glycosidic bond. Under these conditions, the experimental KIEs can be use to approximate the transition state structure.

NAD^+ Methanolysis. In agreement with the results of Oppenheimer,[26] no evidence for CTA-catalyzed NAD^+ methanolysis was obtained. In the presence and absence of CTA, the methanolysis reactions yielded essentially identical HPLC chromatographs, none of which included a methyl-ADP-ribose peak. When the same reactions, with and without CTA, were analyzed by anion exchange chromatography, approximately 0.6% of the applied cpm eluted at 800 mM ammonium bicarbonate, pH 8.0, as expected for ^{14}C-methyl-ADP-ribose. The inability of CTA to catalyze NAD^+ methanolysis is evidence against a covalent, or enzyme-stabilized, enzyme−ADP-ribose intermediate[24] and provides support for a concerted, rather than a stepwise, catalytic mechanism. In addition, the absence of this activity is consistent with the NAD^+ reaction center being neither solvent equilibrated nor solvent accessible at the transition state for CTA-catalyzed NAD^+ hydrolysis.

Magnitudes of the KIEs. The relatively large α-secondary ^{3}H KIE of 1.186 is consistent with a significant increase in bending vibrational freedom of the $C_N1'-H_N1'$ bond. This leads to the predictions that the transition state is dissociative in nature, has sp^2-like hybridization at C_N1' and has a substantially decreased N-glycosidic bond order. The primary ^{15}N KIE, at 1.029, is also consistent with a substantial loss in bond order to nicotinamide. The theoretical maximum for a primary ^{15}N KIE, arising from complete cleavage of a C−N bond, is 1.044.[49,53] At 1.030, the primary ^{14}C KIE is intermediate between the value for a classical S_N1 mechanism (1.00) and that for a symmetric S_N2 mechanism (1.116)[49,53,54] and is consistent with a transition state that is more dissociative than associative. The transition state is predicted to have oxocarbonium ion character, since the ring oxygen donates electron density toward the anomeric carbon in order to stabilize the developing electron deficiency at the reaction center. This results in delocalization of positive charge over the ring $C_N1'-O_N4'$ bond, as well as an increase in $n(C_N1'-O_N4')$.

On the basis of the magnitude of the β-secondary ^{3}H KIE (1.108), the transition state for NAD^+ hydrolysis by CTA is characterized by hyperconjugation within the ribose ring. The hyperconjugation arises from the interaction that occurs between the π-valence orbitals on C_N2' and the developing empty p-orbital on C_N1' when the reaction center is electron deficient. The resulting increase in $n(C_N1'-C_N2')$ further stabilizes the electropositive anomeric carbon. Since some of the C_N2' ground state electron density is recruited into interaction with C_N1', the $C_N2'-H_N2'$ bond gains vibrational freedom and this is manifested in the large, normal H_N2'-^{3}H KIE. Hyperconjugation is predicted to be maximal when the $C_N2'-H_N2'$ and N-glycosidic bonds are eclipsed or nearly-eclipsed,[55] as is the case if the ribosyl ring has a 3′-exo conformation at the transition state.

The inverse and normal H_N4'-^{3}H and H_N5'-^{3}H KIEs, respectively, are indicative of a transition state distortion at positions remote from the reaction center. This distortion increases the vibrational freedom of the $C_N5'-H_N5'$ bond while decreasing that of the $C_N4'-H_N4'$ bond. The exact origin of the inverse H_N4'-^{3}H KIE and the normal H_N5'-^{3}H KIE is unknown. However, comparison with the corresponding KIEs of unity measured for the nonenzymatic reaction indicates that these

(51) Tait, R. M.; Nassau, P. M. *Eur. J. Biochem.* **1984**, *143*, 213−219.
(52) Swain, C. G.; Stivers, E. C.; Reuwer, J. R., Jr.; Schaad, L. J. *J. Am. Chem. Soc.* **1958**, *80*, 5885−5893.
(53) Huskey, W. P. In *Enzyme Mechanism from Isotope Effects*; Cook, P. F., Ed.; CRC Press: Boca Raton, FL, 1991; pp 37−72.
(54) (a) Westheimer, F. H. *Chem. Rev.* **1961**, *61*, 265−273. (b) Fry, A. *Pure Appl. Chem.* **1964**, *8*, 409−419.
(55) Sunko, D. E.; Szele, I.; Hehre, W. J. *J. Am. Chem. Soc.* **1977**, *99*, 5000−5005.

remote KIEs are unique to the enzymatic stabilization of the transition state and arise from specific interactions of the enzyme with the ribose ring.

The observation that the primary KIEs for nonenzymatic NAD^+ hydrolysis are reduced somewhat, relative to those observed with CTA, may be attributed to the effects of solvent. Solvent association may reduce the primary KIEs by causing increases in effective bond order at the electropositive reaction center.[56] The comparatively larger enzymatic primary KIEs suggest that the NAD^+ reaction center may be relatively desolvated when bound in the CTA active site and are consistent with the inability of CTA to catalyze NAD^+ methanolysis.

Transition State Modeling. The starting transition state model incorporated several structural features assumed, on the basis of a qualitative interpretation of the observed KIEs, to characterize the transition state for NAD^+ hydrolysis by CTA. All of the KIEs are consistent with a dissociative transition state having sp^2-like hybridization, and therefore nearly planar geometry, at the anomeric carbon. In addition, the KIEs describe a transition state having substantial oxocarbonium ion character and hyperconjugation within the ribose ring. The ability of CTA to catalyze NAD^+ cleavage in the absence of a specific guanidino compound and the apparent desolvation of NAD^+ in the CTA active site both suggest minimal nucleophilic participation at the transition state.

Ribonolactone was the basis of the starting transition state model because it is sp^2-hybridized at C1. Substitution of a hydrogen atom for the carbonyl oxygen at C1, along with specification of a charge (+1) on the molecule for purposes of structural energy minimization, yields an oxocarbonium ion structure which is planar at the anomeric carbon. In addition, ribonolactone has a 3′-exo ring conformation which, when incorporated into the starting transition state model, brings the $C_N2'-H_N2'$ bond into near alignment with the cleaving N-glycosidic bond. A transition state conformation of this nature is predicted on the basis of the magnitude of the β-secondary ^3H KIE. Finally, since ADP-ribosyl transfer by CTA is known to occur with inversion of configuration at the anomeric carbon,[26] the incoming water nucleophile was modeled as an oxygen atom on the α-face of the NR^+ portion of NAD^+, as in a direct in-line displacement.

From the starting oxocarbonium-ion-like transition state model, bond orders at the reaction center were varied in concert to match the experimentally determined primary and α- and β-secondary KIEs. A family of transition state structures was identified for which all KIEs calculated at the reaction center matched those observed experimentally, within error. For reference, reaction center ground state bond orders are summarized in Figure 2a. The Supporting Information provides a detailed description of the sequential bond order adjustments used to fit the KIEs to a transition state model.

The transition state for NAD^+ hydrolysis by CTA is shown in Figure 2b and reflects bond orders at a value for *f*(deloc) of 1.35. When all reaction center KIEs are fit simultaneously, the allowable range for $n(C_N1'-N_N1)$ is from 0.100 to 0.110 while that for $n(C_N1'-O)$ is from 0.001 to 0.007. These values are consistent with a highly dissociative transition state structure that has sp^2-like hybridization at the anomeric carbon. There is minimal, but required, nucleophilic participation at the transition state, and the bond order to the leaving group is significantly reduced. The structure is also consistent with the predicted oxocarbonium ion character of the transition state. The positive charge developing on the anomeric carbon is delocalized over much of the ribose ring, since the $C_N1'-O_N4'$ bond has double-bond character and causes electron deficiency in neighboring bonds. As predicted from hyperconjugation, the calculated reaction center KIEs are consistent with experimental results when there is an increase in $n(C_N1'-C_N2')$, and a corresponding decrease in $n(C_N2'-H_N2')$. Through hyperconjugation, the positive charge developing on the anomeric carbon is partially delocalized over the $C_N1'-C_N2'$ bond as well.

The remote γ- and δ-secondary ^3H KIEs could be modeled through several variations in the transition state model, all of which were consistent with an enzymatic distortion of the substrate at positions remote from the reaction center. Since a crystal structure of CTA with a bound substrate analog is not yet available, specific enzyme−substrate interactions which might be the origin of the observed remote KIEs have not been established. It may be predicted, however, that recruitment of electron density from ribose hydroxyl groups into hydrogen bonding interactions with the enzyme may result in a movement of the exocyclic C_N5' fragment, an increase in $C_N5'-H_N5'$ vibrational freedom, and the expression of a normal H_N5'-^3H KIE. A calculated H_N5'-^3H KIE very similar to the experimental value was obtained by changing the orientation of the atoms bound to C_N5', relative to the ribose ring, or by increasing the $O_N4'-C_N4'-C_N5'$ bond angle. These results are consistent with a possible anchoring of the C_N5' fragment to the enzyme, resulting in remote distortion of the substrate. The H_N5'-^3H KIE could not be fit by simply rotating the C_N5' fragment or by changing angle bending force constants describing the motion of the $C_N5'-H_N5'$ bond. The inverse H_N4'-^3H KIE may originate in increased strain in the ribose ring as a result of the movement of the C_N5' fragment. A 10% increase in each of the angle-bending force constants describing the motion of the $C_N4'-H_N4'$ bond resulted in calculated H_N4'-^3H KIEs much closer to observed values than those calculated with a 10% decrease in the same angle-bending parameters. In the transition state model (Figure 2b), the $O_N4'-C_N4'-C_N5'$ bond angle is 128°, compared to 107° in the reactant state model. This increase in the $O_N4'-C_N4'-C_N5'$ bond angle reflects the possible magnitude of the distortion necessary to account for the remote KIEs and gives a calculated H_N5'-^3H KIE of 1.030.

Discussion

The CTA Reaction Coordinate and Expression of KIEs. The KIEs measured for NAD^+ hydrolysis by CTA are near-intrinsic and provide direct information on the transition state structure stabilized by the enzyme. The proposed rapid equilibrium random sequential kinetic mechanism for ADP-ribosyl transfer by CTA[13] suggests that NAD^+ binding and dissociation are fast relative to N-glycosidic bond cleavage and is consistent with a small forward commitment factor. The K_m of 14 mM for NAD^+ approximates the K_d in a rapid equilibrium mechanism, and this low substrate affinity is also indicative of a low commitment factor. Forward commitments can often be quantitated by isotope trapping.[57] However, due to the k_{cat} of only 8 min^{-1}, the high K_m for NAD^+, and significant limitations on enzyme solubility, this standard approach could not be used to quantitate forward commitment factors characterizing CTA-catalyzed NAD^+ hydrolysis.

A comparison between enzymatic and nonenzymatic KIEs also provides evidence for the near-intrinsic nature of the KIEs measured on CTA. The KIEs for CTA-catalyzed NAD^+ hydrolysis were compared to those for pH-independent NAD^+ solvolysis, measured at pH 4.0. Above pH 6.5, NAD^+

(56) Burton, G. W.; Sims, L. B.; Wilson, J. C.; Fry, A. *J. Am. Chem. Soc.* **1977**, *99*, 3371−3379.

(57) (a) Rose, I. A. *Methods Enzymol.* **1980**, *64*, 47−83. (b) Rose, I. A. *Methods Enzymol.* **1995**, *249*, 315−340.

solvolysis becomes pH-dependent and base-catalyzed.[30] Considering only the magnitude of the α-secondary ^{3}H KIE for CTA-catalyzed NAD^+ hydrolysis, nucleophilic catalysis can be eliminated as a possible mechanism. Therefore, pH-independent NAD^+ hydrolysis was chosen as the nonenzymatic reaction model. However, the α-secondary ^{2}H KIE for base-catalyzed NAD^+ solvolysis indicates that a dissociative transition state characterizes this reaction as well.[29]

The families of KIEs measured for CTA-catalyzed and nonenzymatic NAD^+ hydrolysis display similar magnitudes for individual isotope effects. While the particular differences noted in a comparison of the individual enzymatic and solution KIEs provide information on unique contributions of the enzyme to transition state stabilization, the overall similarity is most simply interpreted as resulting from similar reaction coordinates that are both characterized by a single, rate-limiting transition state at which N-glycosidic bond cleavage occurs. Thus, it is likely that the equilibrium between the ground state and the transition state, required for full expression of KIEs, is not obscured by any substantial forward commitment of NAD^+ to catalysis and that the KIEs observed on CTA are near-intrinsic.

Additional evidence exists to suggest that CTA catalyzes NAD^+ hydrolysis and ADP-ribosyl transfer through a concerted mechanism. For example, CTA catalyzes ADP-ribosyl transfer with inversion of configuration at the anomeric carbon[26] but does not catalyze NAD^+ methanolysis[26] (and this work). In addition, the formation of a stabilized, or perhaps covalent, enzyme−ADP-ribose intermediate has not been detected in CTA-catalyzed NAD^+ hydrolysis or ADP-ribosyl transfer.[12,24]

The small, inverse solvent deuterium KIE demonstrates that the CTA reaction coordinate is not characterized by a rate-limiting proton transfer. The solvent KIE also provides evidence against a diol anion mechanism in CTA catalysis. It has been proposed that both enzymatic and pH-dependent, base-catalyzed NAD^+ hydrolysis proceed through an oxocarbonium-ion-like transition state that is characterized by a diol anion involving the 2′- and 3′-hydroxyl groups of the nicotinamide ribose.[30,58] Formation of the ribose diol anion requires partial transfer and sharing of a proton between the hydroxyl oxygens and between a hydroxyl oxygen and the active site carboxylate. Proton transfer at the transition state would result in a large, normal solvent deuterium KIE.

The expression relating intrinsic KIEs to observed KIEs[59] is as follows:

$$^{D}(V/K) = (^{D}k + c_f + c_r{}^{D}K_{eq})/(1 + c_f + c_r)$$

where $^{D}(V/K)$ is the observed KIE (a deuterium KIE in this example), c_f is the forward commitment factor, c_r is the reverse commitment factor, $^{D}K_{eq}$ is the equilibrium isotope effect, and ^{D}k is the intrinsic KIE. Since NAD^+ hydrolysis is irreversible ($\Delta G = -8.2$ kcal/mol),[19] c_r is likely to be negligible. The above expression then reduces to

$$^{D}(V/K) = (^{D}k + c_f)/(1 + c_f)$$

The α-secondary ^{3}H KIE for pH-independent, water-catalyzed NAD^+ hydrolysis, at 1.238, is likely to be the practical upper limit for the KIE at this position. If a c_f of 0.30 is assumed, the intrinsic enzymatic H_N1'-^{3}H KIE is 1.242 and is in excess of that observed for the nonenzymatic reaction. This analysis indicates that c_f is smaller than 0.3 for CTA-catalyzed NAD^+ hydrolysis. With the exception of the α- and β-secondary ^{3}H KIEs, adjustment of the enzymatic KIEs for a c_f of 0.20 is within the range of experimental error. Given the evidence presented above, from both steady-state kinetics and comparison of enzymatic and nonenzymatic KIEs, the value of c_f that characterizes the CTA-catalyzed NAD^+ hydrolysis is below 0.20. Correction for a c_f below 0.20 yields KIEs that are similar to those observed and thus produces a transition state model with features closely related to that presented.

KIEs at the Reaction Center. The family of KIEs measured for NAD^+ hydrolysis by CTA is consistent with an enzymatic mechanism characterized by nearly unimolecular N-glycosidic bond cleavage. The development of oxocarbonium ion character within the ribose ring can be visualized by comparing the electrostatic potential surface areas of the reactant and transition state models, as shown in Figure 4. The qualitative nature of the transition state can be derived from the large H_N1'-^{3}H KIE (1.19), which is diagnostic for a dissociative transition state since it originates in the increased bending vibrational freedom of the $C_N1'-H_N1'$ bond.[48,49] The sp^2-like hybridization at the anomeric carbon, and the requisite development of positive charge in the ribose ring as the bond to nicotinamide is cleaved, correlates with oxocarbonium ion character at the transition state. The oxocarbonium ion character is described by delocalization of positive charge over the ribose ring and by an increase in $n(C_N1'-O_N4')$. The primary ^{15}N KIE is uniquely dependent on N-glycosidic bond order and, at 1.03, is relatively large compared to the maximal value of 1.04 predicted for complete loss of N-glycosidic bond order at the transition state.[49,53] Thus, the N_N1-^{15}N KIE is consistent with a highly dissociative transition state having substantially decreased bond order to the leaving group nicotinamide.

The large, normal H_N2'-^{3}H KIE of 1.11 is diagnostic for hyperconjugation within the ribose ring at the transition state and rules out a classical S_N2 displacement at C_N1'. The increased vibrational freedom of the $C_N2'-H_N2'$ bond correlates with recruitment of C_N2' electron density out of this bond and into interaction with the developing empty p-orbital on the electron-deficient anomeric carbon. Like the interaction between the ring oxygen and the anomeric carbon at the transition state, the net effect of hyperconjugation is to stabilize the electropositive reaction center by intramolecular donation of bond order, thereby further delocalizing the positive charge through the ribose ring. Approximately 5% of the additional intramolecular bond order at the transition state is localized to the $C_N1'-C_N2'$ bond. The magnitude of the β-secondary ^{3}H KIE requires a small $N_N1-C_N1'-C_N2'-H_N2'$ dihedral angle at the transition state, facilitating hyperconjugative stabilization.[55] The orbital overlaps causing this isotope effect may only be achieved by an alteration in ribose ring pucker, from 3′-endo in the ground state to 3′-exo at the transition state.

The primary ^{14}C KIE is a direct function of reaction coordinate motion and reports on the overall nature of the transition state. At 1.03, the C_N1'-^{14}C KIE is consistent with a transition state that is more dissociative than associative, based on comparison with the theoretical range of primary ^{14}C KIEs, from 1.00 for a classical S_N1 mechanism to 1.12 for a symmetric S_N2 mechanism.[49,53,54,60] Relative to a symmetric S_N2 transition state, increasingly unbalanced forces on the anomeric carbon lead to increased transition state fractionation factors. The net effect is a reduction of the primary ^{14}C KIE from the theoretical

(58) Handlon, A. L.; Xu, C.; Muller-Steffner, H. M.; Schuber, F.; Oppenheimer, N. J. *J. Am. Chem. Soc.* **1994**, *116*, 12087−12088.

(59) Northrop, D. B. *Annu. Rev. Biochem.* **1981**, *50*, 103−131.

(60) Melander, L.; Saunders, W. H., Jr. In *Reaction Rates of Isotopic Molecules;* John Wiley & Sons: New York, 1980; pp 225−257. Rehybridization of the anomeric carbon C_N1' toward sp^2 in the transition state makes a p-orbital available to form a π-bond-like interaction with C_N2' and with the ring oxygen O_N4'. These interactions could not be formed in the ground state because of the sp^3-hybridized C_N1'.

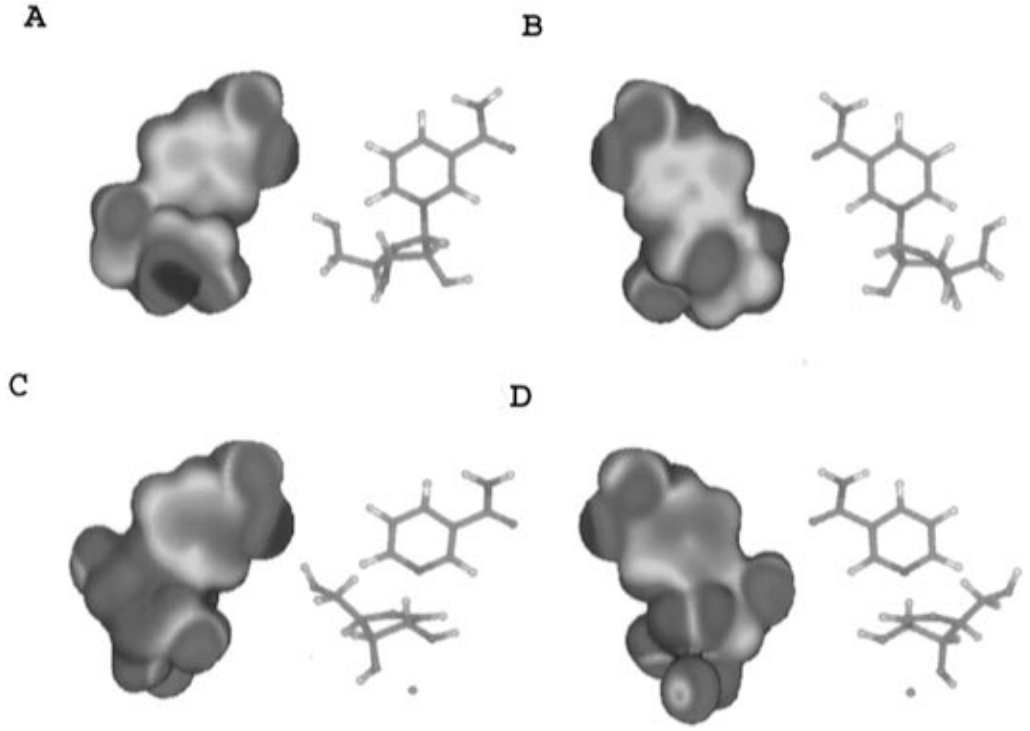

Figure 4. Electrostatic potentials at the molecular surfaces of reactant NAD^+ and the transition state for CTA-catalyzed NAD^+ hydrolysis. The potentials are presented at an electron density of 0.002 e/*b*.[3] A and B represent front and back views of the nicotinamide−ribose portion of substrate, while C and D are the transition state. In each case, the electron density and electrostatic potentials are calculated with the *CUBE* function of *Guassian 94*. Visualization of the surfaces is through the *AVS Chemistry Viewer* (Advanced Visual Systems Inc. and Molecular Simulations Inc.). The color blue represents electron-rich regions, and red indicates relative electron deficiencies. Both substrate and transition state carry a net +1 charge. The corresponding stick figures were created with the Insight II package (Biosym/MSI), and here green indicates carbon atoms, red indicates the oxygens, blue indicates the nitrogens, and white indicates the hydrogen atoms. The partial positive charge of the nicotinamide is broadly distributed over the conjugated ring. At the transition state, the positive charge migrates from the nicotinamide to the ribose. The reactant molecule (A and B) has a net charge distribution of 0.58 and 0.42 on the ribosyl and nicotinamide groups, respectively. The charge distribution shifts to 0.84 and 0.16 on the ribosyl and nicotinamide groups in the transition state. The incipient nucleophilic oxygen atom is shown as a charge-neutral group in these calculations and is shown only in C and D.

maximum to one characteristic of a more dissociative transition state. A dissociative transition state may also be characterized by intramolecular donation of bond order to stabilize the electropositive reaction center.[60] This is true of the transition state for CTA-catalyzed NAD^+ hydrolysis, given the evidence for hyperconjugation and oxocarbonium ion character in the ribose ring. The increased bond order at the anomeric carbon, which counteracts the effect of the bond order loss between the anomeric carbon and the leaving group, may further suppress the primary ^{14}C KIE from the theoretical maximum.

BEBOVIB modeling of the reaction center KIEs confirms that the transition state for NAD^+ hydrolysis by CTA is highly dissociative. To obtain the transition state structure, bond orders to the incoming water nucleophile and the leaving group nicotinamide were varied while adjusting the connected bonds in the ribose according to equations 1−3. The effects of varying the values for *f*(deloc) and *p* (eqs 1 and 2) were explored at a variety of positions along the reaction coordinate, defined by the extent of bond cleavage and formation at the anomeric carbon. The primary ^{15}N KIE was fit at a $C_N1'-N_N1$ bond order of approximately 0.1 and was essentially insensitive to the values of *f*(deloc) and *p* used to describe bond order within the ribose ring. In contrast, the calculated primary ^{14}C KIE was highly sensitive to the amount of additional intramolecular bond order delocalized within the ribose reaction center and was also influenced somewhat by the particular distribution of this bond order. The magnitude of the β-secondary ^3H KIE defined this distribution, localizing approximately 95% of the additional intramolecular bond order to the $C_N1'-O_N4'$ bond and about 5% to the $C_N1'-C_N2'$ bond. The magnitude of the α-secondary ^3H KIE allowed definition of the range of *f*(deloc) values providing chemically reasonable transition state models. The $C_N1'-H_N1'$ bond order is expected to increase somewhat as the anomeric carbon rehybridizes from sp^3 to sp^2-like at the transition state. Given these constraints imposed on the transition state model, a bond order to the incoming nucleophile of less than 1% was required to model the primary ^{14}C KIE.

The family of transition state models, for which all calculated KIEs match experimentally determined values, is characterized by values for *f*(deloc) in the range of 1.30−1.45. Thus, the modeling required that the amount of bond order delocalized into the ribose ring be greater than the net loss in bond order to the leaving group. While the particular values for *f*(deloc) required to fit the observed KIEs are a function of the N-glycosidic bond order in the ground state model, the *f*(deloc) parameter actually accounts for the expected increase in total bond order to the electropositive anomeric carbon as a result of the increased availability of π-bond-like interactions within the ribose ring. This is characteristic of oxocarbonium ion reaction centers.[60] In order to model the reaction center KIEs for CTA-catalyzed NAD^+ hydrolysis, *f*(deloc) required a value greater than unity. The total bond order at C_N1' at the transition state is 4.0, compared to 3.8 for the reactant state.

Although the bond order between the anomeric carbon and the incoming water nucleophile is less than 1% at the transition state, nucleophilic participation is required to fit the calculated KIEs to those observed, given the coupled vibrational modes and interaction force constants used. Substantial nucleophilic participation at the transition state for NAD^+ hydrolysis by CTA is not expected since CTA, as an ADP-ribosyltransferase, can

activate the substrate in the absence of a specific guanidino compound and can therefore catalyze essentially unimolecular N-glycosidic bond cleavage. However, while the water nucleophile does not strongly participate in the chemistry, it is poised to react with the oxocarbonium-ion-like transition state. This is consistent with studies of model systems showing that a glycosyl oxocarbonium ion has a lifetime of about 10^{-12} s and is on the borderline of being too unstable to form in the absence of nucleophilic preassociation.[61] As a further example, NAD^+ solvolysis in mixtures of methanol and water yields methylated-ADP-ribose and ADP-ribose at a ratio that depends only on the mole fraction of methanol and not on its relative nucleophilicity.[24] The oxocarbonium ion transition state does not become solvent equilibrated but instead reacts with the solvent molecule poised at the proper position in the solvation shell surrounding the reaction center.

A gas phase study of NR^+ hydrolysis, with inversion of configuration at the anomeric carbon, indicates that the approach of the incoming nucleophile does not become energetically favorable until the bond order to nicotinamide is about 10%.[62,63] This result is consistent with the requirement for bond order to the incoming nucleophile at the transition state and also agrees well with the N-glycosidic bond order of approximately 10% predicted for the transition state structure presented here.

Contributions of CTA to Transition State Stabilization. Work on the general mechanism of enzymatic NAD^+ hydrolysis has focused on NAD^+ glycohydrolases from *N. crassa*, porcine brain, and calf spleen. Each of these enzymes stabilizes a dissociative, electropositive transition state for N-glycosidic bond cleavage. This is shown by the α-secondary ^{2}H KIEs of 1.100 and 1.132 for NMN^+ hydrolysis by *N. crassa* and porcine brain NAD^+ glycohydrolases, respectively,[28] as well as by the β_{lg} of −0.90 for hydrolysis of pyridinium analogs of NAD^+ by calf spleen NAD^+ glycohydrolase.[31] Given the reactivity of the N-glycosidic bond of NAD^+,[64] a dissociative transition state may be a general feature of the reaction coordinates of enzymes catalyzing NAD^+ cleavage reactions. Acid or base catalysis are unlikely as explanations of the mechanism of enzymatic NAD^+ hydrolysis considering the cationic nature of the leaving group and the large magnitude of the α-secondary KIE. Catalysis by strain or distortion of the substrate has also been suggested[28] but is considered unlikely, since studies of calf spleen NAD^+ glycohydrolase have not provided evidence for the tight binding at either end of the scissile bond that may be required for converting binding energy into labilization of the N-glycosidic bond.[31,58,63,65] For example, 2′-substituted ribose analogs of NAD^+ are hydrolyzed at rates reflecting only the relative stability of the oxocarbonium ion transition state.[58] Differential electrostatic stabilization of the reactant and transition states may contribute to catalysis of NAD^+ hydrolysis since positive charge shifts to the ribosyl ring in the transition state (Figure 4).

CTA is mechanistically similar to other NAD^+ glycohydrolases in also stabilizing a dissociative, electropositive transition state. Analysis of the family of KIEs measured for NAD^+ hydrolysis by CTA leads to some suggestions regarding the possible origin of the catalytic power of NAD^+-hydrolyzing enzymes. CTA may labilize the N-glycosidic bond of NAD^+ by desolvating the reaction center at the enzyme active site. Attainment and stabilization of the transition state may then be facilitated by enzyme-induced distortion of the substrate at positions remote from the reaction center. Further stabilization of the oxocarbonium-ion-like transition state may be derived from electrostatic interaction with an active site carboxylate, Glu112, which has been shown to be essential for catalysis.[66,67]

Substrate destabilization by desolvation has previously been proposed to characterize enzymatic NAD^+ hydrolysis.[63] Gas phase studies of the collisionally-activated dissociation of 2′-substituted nicotinamide arabinosides[68] have shown that removal of solvent molecules from the nucleoside reaction center, as in a monomolecular dispersion in a vacuum, leads to dissociation of the nucleoside into nicotinamide and an oxocarbonium ion. In the absence of solvent, there is essentially no possibility for recombination of the oxocarbonium ion with the leaving group.[63]

The inability of CTA to catalyze NAD^+ methanolysis is evidence that the NAD^+ reaction center is relatively desolvated when bound in the enzyme active site. By extension, the water nucleophile participating in NAD^+ hydrolysis may be enzyme-associated. This water molecule may be activated by the CTA active site residue His44.[69] Activation of the water nucleophile by His44 may be the origin of the slightly inverse solvent deuterium KIE. However, inverse solvent KIEs of similar magnitudes have, in some cases, been attributed to the effects of solvent viscosity.[70]

In addition, the apparent relative suppression of the primary ^{15}N and ^{14}C KIEs in solution, relative to those observed on the enzyme, may also indicate that the NAD^+ reaction center is relatively desolvated at the enzyme active site. In solution, reaction center solvation may stabilize the oxocarbonium ion transition state by generally increasing bond order in the vicinity of the N-glycosidic bond.[56] In the CTA active site, the energetically unfavorable exclusion of solvent molecules from the reaction center may enhance the reactivity of the N-glycosidic bond and thereby decrease the activation barrier for attaining the transition state. Perhaps guanidino compounds that are ADP-ribosylated by CTA have a specific site of association to the enzyme that allows them access to the otherwise solvent inaccessible reaction center.

Through specific enzyme−substrate interactions, CTA may attain and stabilize the transition state for NAD^+ hydrolysis by distorting the substrate at positions remote from the reaction center. The γ- and δ-secondary ^{3}H KIEs are measured at positions remote from the reaction center, and their expression reflects transition state distortions in the ribose ring that do not occur in NAD^+ solvolysis. The normal H_N5'-^{3}H KIE can be modeled by distorting the conformation of atoms on C_N5', relative to the ribose ring. An appropriate distortion can be achieved by increasing the $O_N4'-C_N4'-C_N5'$ bond angle and

(61) Amyes, T. L.; Jencks, W. P. *J. Am. Chem. Soc.* **1989**, *111*, 7888−7900.
(62) Schröder, S.; Buckley, N.; Oppenheimer, N. J.; Kollman, P. A. *J. Am. Chem. Soc.* **1992**, *114*, 8232−8238.
(63) Oppenheimer, N. J. *Mol. Cell. Biochem.* **1994**, *138*, 245−251.
(64) Oppenheimer, N. J. In *Pyridine Nucleotide Coenzymes. Chemical, Biochemical, and Medical Aspects; Coenzymes and Cofactors*; Dolphin, D., Poulson, R., Avramovic, O., Eds.; John Wiley & Sons: New York, 1987; Vol. II, Part A, pp 323−365.
(65) Schuber, F.; Travo, P.; Pascal, M. *Bioorg. Chem.* **1979**, *8*, 83−90.
(66) (a) Tsuji, T.; Inoue, T.; Miyama, A.; Noda, M. *FEBS Lett.* **1991**, *291*, 319−321. (b) Tsuji, T.; Inoue, T.; Miyama, A.; Okamoto, K.; Honda, T.; Miwatani, T. *J. Biol. Chem.* **1990**, *265*, 22520−22525.
(67) Lobet, Y.; Cluff, C. W.; Cieplak, W., Jr. *Infect. Immun.* **1991**, *59*, 2870−2879.
(68) Buckley, N.; Handlon, A. L.; Maltby, D.; Burlingame, A. L.; Oppenheimer, N. J. *J. Org. Chem.* **1994**, *59*, 3609−3615.
(69) (a) Jobling, M. G.; Connell, T. D.; Holmes, R. K. In *Proceedings of Cholera Toxin and Related Enterotoxins, From Disease to Molecular Structure*; Worcestershire, 1993; pp 33−34. (b) Burnette, W. N.; Cieplak, W., Jr.; Kaslow, H. R.; Rappuoli, R.; Tuomanen, E. In *Recombinant Microbes for Industrial and Agricultural Applications*; Murooka, Y., Imanaka, T., Eds.; Marcel Dekker, Inc.: New York, 1994; pp 185−203. (c) Antoine, R.; Locht, C. *J. Biol. Chem.* **1994**, *269*, 6450−6457.
(70) Karsten, W. E.; Lai, C.-J.; Cook, P. F. *J. Am. Chem. Soc.* **1995**, *117*, 5914−5918.

thereby altering the relative position of the entire C_N5' fragment. The increase in this bond angle is consistent with a possible anchoring of the C_N5' fragment to the enzyme through specific hydrogen-bonding interactions between CTA and substrate hydroxyl groups. On the basis of the crystallographic information currently available on CTA,[3,71,72] the identities of the active site residues potentially involved in this substrate distortion have not been established. Of the residues in direct contact with NAD^+ in the crystal structure of diphtheria toxin with NAD^+ bound, only two are conserved in the heat-labile enterotoxin from *E. coli*.[72] One of the conserved residues is a Gly and the other is the active site Glu. The ability to model the inverse H_N4'-^3H KIE by increasing angle-bending strain within the ribose ring is consistent with the proposed movement of the C_N5' fragment.

Thus, a model for catalysis of NAD^+ hydrolysis by CTA may involve labilization of the ground state by reaction center desolvation. The transition state may then be attained and stabilized by specific anchoring of substrate hydroxyl group(s) to the enzyme through hydrogen-bonding interactions. The resulting distortion may contribute to alteration of the ribose ring pucker from 3′-endo in the reactant to the activated 3′-exo conformation of the oxocarbonium-ion-like transition state. The electropositive transition state may also be electrostatically stabilized by the active site carboxylate, Glu112. This combination of ground state destabilization, substrate activation, and transition state stabilization may lead to the expulsion of nicotinamide from NAD^+ in the presence of weak nucleophilic participation.

The oxocarbonium ion character of the transition state stabilized by CTA may be less extensively developed than that for NAD^+ hydrolysis in solution. The participation of active site residues in stabilizing the transition state for CTA-catalyzed NAD^+ hydrolysis prevents formation of a fully developed oxocarbonium ion. Evidence for enzymatic stabilization of a relatively early transition state is derived from the comparatively low enzymatic α- and β-secondary ^3H KIEs. The out-of-plane bending vibrational freedom of the $C_N1'-H_N1'$ bond does not increase as extensively on the enzyme as it does in solution, indicating relatively less sp^2-like hybridization at the anomeric carbon. In addition, CTA active site residues apparently dictate a charge distribution within the ribose ring that differs from that in solution. The relatively small β-secondary ^3H KIE observed for CTA-catalyzed NAD^+ hydrolysis suggests that perhaps CTA active site residues stabilize the transition state in a manner that diminishes the need for hyperconjugative redistribution of positive charge over the $C_N1'-C_N2'$ bond, relative to the solution reaction. The $N_N1-C_N1'-C_N2'-H_N2'$ dihedral angle may be less compressed on the enzyme, compared to that of the transition state in solution. Additional information regarding the details of the transition state structure for CTA-catalyzed NAD^+ hydrolysis, as well as the unique manner in which CTA stabilizes this transition state, may be gained following BEBOVIB modeling of the transition state for NAD^+ solvolysis.

Transition State Structure Based Inhibitor Design. Few potential transition state analog inhibitors are available for ADP-ribosyltransferases such as CTA. Adenosine diphosphate dihydroxypyrrolidine inhibits NAD^+ glycohydrolase from *Bungarus fasciatus* venom with a K_i of 94 μM ($K_{m(NAD^+)} = 14$ μM).[73,74] However, this compound does not inhibit NAD^+ hydrolysis by porcine brain NAD^+ glycohydrolase or diphtheria toxin.[74] ADP-ribonolactone inhibits calf spleen NAD^+ glycohydrolase with a K_i of 115 μM ($K_{m(NAD^+)} = 56$ μM).[21,75] An effective transition state analog inhibitor of dissociative, enzymatic NAD^+ hydrolysis has not yet been developed.

With the model presented here for the complete transition state structure stabilized during CTA-catalyzed NAD^+ hydrolysis, it is possible to design stable molecules incorporating the geometric and electrostatic properties of the transition state. A series of potentially useful compounds has been synthesized on the basis of the transition state for inosine hydrolysis by nucleoside hydrolase from *Crithidia fasciculata*.[33,34,42] This enzyme stabilizes a transition state similar to that presented here. The most potent inhibitors available for nucleoside hydrolase are 1(*S*)-phenyl-1,4-dideoxy-1,4-iminoribitol ($K_i = 30$ nM, $K_{m(inosine)} = 380$ μM)[76] and (*p*-nitrophenyl)riboamidrazone ($K_i = 2$ nM). These compounds were not effective inhibitors of CTA catalysis. Therefore, coupling of the ADP structure to the nucleoside hydrolase inhibitors may be necessary for binding recognition by CTA.

On the basis of alignment with the crystal structure of diphtheria toxin with NAD^+ bound,[72] Arg7 of CTA is predicted to interact with either the ribose or phosphate of the AMP portion of NAD^+. Arg7 is critical to substrate binding and catalysis and even a relatively conservative substitution to Lys is not tolerated.[67,77] Thus, binding interactions with Arg7 are almost certainly required for substrate or inhibitor recognition. Transition state structure based inhibitors of catalysis by CTA could be useful as an orally administered treatment for cholera.

Acknowledgment. This work was supported by NIH Research Grant AI34342, Training Grant 5T32GM07260, and assistance from the G. Harold and Leila Y. Mathers Charitable Foundation. The kinetic isotope effects for nonenzymatic NAD^+ hydrolysis were determined in cooperation with Dr. Paul J. Berti. The authors thank Dr. Benjamin A. Horenstein and Dr. Paul J. Berti for advice on the transition state modeling process and Dr. Carey Bagdassarian for preparing Figure 4.

Supporting Information Available: Details of the BEBOVIB modeling of the transition state structure for CTA-catalyzed NAD^+ hydrolysis (4 pages). See any current masthead page for ordering and Internet access instructions.

JA9621915

(71) (a) Sixma, T. K.; Kalk, K. H.; van Zanten, B. A. M.; Dauter, Z.; Kingma, J.; Witholt, B.; Hol, W. G. J. *J. Mol. Biol.* **1993**, *230*, 890−918. (b) Sixma, T. K.; Pronk, S. E.; Kalk, K. H.; Wartna, E. S.; van Zanten, B. A. M.; Witholt, B.; Hol, W. G. J. *Nature* **1991**, *351*, 371−377.

(72) Bell, C. E.; Eisenberg, D. *Biochemistry* **1996**, *35*, 1137−1149.

(73) Yost, D. A.; Anderson, B. M. *J. Biol. Chem.* **1981**, *256*, 3647−3653.

(74) Slama, J. T.; Simmons, A. M.; Hassan, M. E.; Aboul-Ela, N.; Jacobson, M. K. In *ADP-Ribosylation Reactions*; Poirier, G. G., Moreau, P., Eds.; Springer-Verlag: New York, 1992; pp 316−320.

(75) Schuber, F.; Pascal, M. *FEBS Lett.* **1977**, *73*, 92−96.

(76) Parkin, D. W.; Horenstein, B. A.; Abdulah, D. R.; Estupiñán, B.; Schramm, V. L. *J. Biol. Chem.* **1991**, *266*, 20658−20665.

(77) Burnette, W. N.; Mar, V. L.; Platler, B. W.; Schlotterbeck, J. D.; McGinley, M. D.; Stoney, K. S.; Rohde, M. F.; Kaslow, H. R. *Infect. Immun.* **1991**, *59*, 4266−4270.